NeuroImage 195 (2019) 475–489

Contents lists available at ScienceDirect

NeuroImage

journal homepage: www.elsevier.com/locate/neuroimage

Self-directed down-regulation of auditory cortex activity mediated by real-time fMRI neurofeedback augments attentional processes, resting cerebral perfusion, and auditory activation

Matthew S. Sherwood [a,*], Jason G. Parker [b], Emily E. Diller [b,c], Subhashini Ganapathy [a,d], Kevin B. Bennett [e], Carlos R. Esquivel [f], Jeremy T. Nelson [b,f,g]

[a] Department of Biomedical, Industrial & Human Factors Engineering, Wright State University, Dayton, OH, USA
[b] Department of Radiology and Imaging Sciences, Indiana University School of Medicine, Indiana University, IN, USA
[c] College of Health and Human Services, Purdue University, West Lafayette, IN, USA
[d] Department of Trauma Care, Boonshoft School of Medicine, Wright State University, Dayton, OH, USA
[e] Department of Psychology, Wright State University, Dayton, OH, USA
[f] Department of Defense Hearing Center of Excellence, JBSA-Lackland, USA
[g] Ho-Chunk Inc., Alexandria, VA, USA

ARTICLE INFO

Keywords:
fMRI
Neurofeedback
Neuromodulation
Primary auditory cortex
Attention
Tinnitus

ABSTRACT

In this work, we investigated the use of real-time functional magnetic resonance imaging (fMRI) with neurofeedback training (NFT) to teach volitional down-regulation of the auditory cortex (AC) using directed attention strategies as there is a growing interest in the application of fMRI-NFT to treat neurologic disorders. Healthy participants were separated into two groups: the experimental group received real feedback regarding activity in the AC; the control group was supplied sham feedback yoked from a random participant in the experimental group and matched for fMRI-NFT experience. Each participant underwent five fMRI-NFT sessions. Each session contained 2 neurofeedback runs where participants completed alternating blocks of "rest" and "lower" conditions while viewing a continuously-updated bar representing AC activation and listening to continuous noise. Average AC deactivation was extracted from each closed-loop neuromodulation run and used to quantify the control over AC (AC control), which was found to significantly increase across training in the experimental group. Additionally, behavioral testing was completed outside of the MRI on sessions 1 and 5 consisting of a subjective questionnaire to assess attentional control and two quantitative tests of attention. No significant changes in behavior were observed; however, there was a significant correlation between changes in AC control and attentional control. Also, in a neural assessment before and after fMRI-NFT, AC activity in response to continuous noise stimulation was found to significantly decrease across training while changes in AC resting perfusion were found to be significantly greater in the experimental group. These results may be useful in formulating effective therapies outside of the MRI, specifically for chronic tinnitus which is often characterized by hyperactivity of the primary auditory cortex and altered attentional processes. Furthermore, the modulation of attention may be useful in developing therapies for other disorders such as chronic pain.

1. Introduction

The rapidly growing field of neuromodulation technology gives rise to promising technology to treat the neurologic disorders by utilizing the ability to induce and/or control neural plasticity (Johnston et al., 2011; Veit et al., 2012) and combating brain disorders and diseases (Hamilton et al., 2011; Vaughan et al., 2006). Of the techniques currently being explored, endogenous neuromodulation techniques

Abbreviations: EV, explanatory variable; NFT, neurofeedback training; AC, auditory cortex; A1, primary auditory cortex; CPT-X, continuous performance task; AE, attention to emotion task; pcASL, pseudo-continous arterial spin labeling.

* Corresponding author. Wright State University, 413 Neuroscience Engineering Collaboration, 3640 Colonel Glenn Highway, Dayton, OH, 45435, USA.
E-mail address: matt.sherwood@wright.edu (M.S. Sherwood).

https://doi.org/10.1016/j.neuroimage.2019.03.078
Received 24 May 2018; Received in revised form 23 February 2019; Accepted 31 March 2019
Available online 5 April 2019

(Mak and Wolpaw, 2009; Smith et al., 2004; Sulzer et al., 2013) have the advantages of no known side effects and may be translated to exercises that could be performed at home without the use of sophisticated equipment and trained professionals (Caria et al., 2007; Linden et al., 2012). Real-time functional magnetic resonance imaging (Cox et al., 1995; Weiskopf et al., 2007) has seen a dramatic rise in interest since its advent in 1995, with a large portion of research dedicated to its application for training endogenous neuromodulation. In this technique, termed closed-loop endogenous neuromodulation, the functional magnetic resonance imaging (fMRI) signal is measured from a specific region of the brain, processed, and presented to the subject in real-time (*i.e.,* neurofeedback). Through training, subjects develop self-directed mental processing techniques that regulate this signal.

One such focus of fMRI neurofeedback training (fMRI-NFT) is on the treatment of tinnitus. Tinnitus, the phantom perception of sound, is associated with emotional distress including anxiety and depression that can have a profound effect on mental health and overall quality of life (Halford and Anderson, 1991; Jun and Park, 2013), and was the main motivation of this work. The neural mechanisms of tinnitus are not well understood but have been studied using various techniques. Although there is no cure for tinnitus, there is a rapidly-expanding portfolio of treatment options that include pharmacologic, behavioral, and neuromodulatory strategies. Tinnitus treatments are categorized almost universally as treating 1) the tinnitus percept (*i.e.,* the neural mechanisms responsible for the rise of the percept) or 2) the tinnitus affect (*i.e.,* the emotional response). Pharmacologic and behavioral therapies make up the majority of treatment strategies for tinnitus patients, but both currently target the tinnitus affect.

Neuromodulatory techniques attempt to correct abnormal neural patterns of the brain. In the case of tinnitus, the target is often the auditory cortex (AC), which has been shown to be hyperactive in fMRI studies (Gu et al., 2010; Seydell-Greenwald et al., 2012) and have elevated steady-state metabolism in positron emission tomography studies (Langguth et al., 2006; Schecklmann et al., 2013; Wang et al., 2001). Using fMRI-NFT, internal stimulation is utilized to potentially target either the tinnitus percept or affect (Folmer et al., 2014). Three previous studies have investigated the effect of control over the activation of the AC learned from fMRI-NFT on is achievable without concurrent auditory stimulation during attempted control. In the first controlled study, it was indicated that healthy individuals can learn to control the activated cortical volume in the primary and secondary auditory cortex using fMRI-NFT (Yoo et al., 2006). In the second study, it was reported that control over the magnitude of A1 activation is achievable in a cohort of tinnitus patients (Haller et al., 2010). However, this study was not controlled so this finding could not be necessarily attributable to fMRI-NFT and subjective measures of tinnitus were not statistically analyzed. More recently, Emmert et al. (2017a,b) demonstrated the capacity of tinnitus patients to down-regulate the auditory cortex using continuous and intermittent neurofeedback. Single-session results identified greater down-regulation in the intermittent feedback group; but over multiple sessions, the continuous feedback was more advantageous. There were no reported changes in resting cerebral blood perfusion within the auditory cortex; however, there was a significant decrease in the relaxtion sub-score of the tinnitus functional index indicating relaxation capacity was less impacted by tinnitus.

In the work presented here, we translated our previous work investigating control over the prefrontal cortex using fMRI-NFT and cognitive abilities (Sherwood et al., 2016a, 2016b) to teach volitional down-regulation of the AC during binaural auditory stimulation using directed attention strategies. Our goal of this work is to demonstrate the possibility of subjects to endogenously down-regulate AC activity in the presence of a controlled stimulus and relate this to behavior; therefore, healthy subjects were selected for this study.

2. Methods

2.1. Participants

This study utilized healthy volunteers recruited from Wright State University and the surrounding community. Each participant completed a telephone screening to qualify for the study. Forty-one participants randomly selected from the qualifying pool were enrolled for further screening. Written informed consent was obtained from each participant prior to any experimental procedures which were approved by Wright State University's Institutional Review Board (IRB) and the Air Force Medical Support Agency Surgeon General's Research Oversight Committee. Participants that were eligible for compensation received equal remuneration.

The participants were randomly assigned to one of two groups. Both groups received the same instructions and performed the same tasks with the exception of the authenticity of the feedback during endogenous closed-loop neuromodulation. In the experimental group (EXP), real feedback was provided while sham feedback was utilized in the control group (CON). Participants in each group were blinded to the validity of the feedback. In total, thirteen (4 CON, 9 EXP) participants voluntarily withdrew for unknown reasons or were withdrawn from the study due to excessive motion, absenteeism/tardiness, or software/hardware issues that limited the completion of study procedures. Of these thirteen, 6 (3 CON) gave written, informed consent but did not complete any experimental sessions, four (1 CON) were removed after a single session due to excessive motion (3) or unknow reasons (1), two participants were withdrawn after 2 sessions, and the last participant was withdrawn after 4 sessions due to the inability to complete the fifth session within the 21-day timeframe. Furthermore, the MRI data for a single EXP participant was corrupted and excluded from the analysis. The presented results represent the remaining twenty-seven participants: eighteen EXP participants (mean age 23.2 $\pm$ 1.1, 11 males) and nine CON participants (mean age 24.4 +/2.5, 4 males). This imbalance was maintained by design to complete the objectives of the funded work while maintaining a controlled design to properly evaluate the effects of the study.

2.2. Experimental design

An overview of the experimental design is shown in Fig. 1. All participants first completed a preliminary visit where informed consent was obtained. After consenting to the experiment, the participants completed a few demographic forms and a standard MRI screening form. Prior to familiarizing the participants with the testing apparatus, a short hearing test was conducted using a mobile audiometry system (Shoebox Audiometry, Ontario, Canada) with calibrated transducers (HDA 280, Sennheiser, Wedemark, Deutschland). This was conducted in a standard laboratory setting to verify normal hearing, determined by no frequencies with a hearing threshold above 40 dB on a standard audiogram to ensure a normal, healthy auditory system. The implemented hearing test was a simple, self-applied examination that has been clinically validated (Saliba et al., 2016; Thompson et al., 2015).

The remaining experimental procedures were completed across five sessions completed within 21 days and no more than one per day. The first session began with a behavioral assessment followed by an assessment of neural measures and fMRI-NFT. The second, third, and fourth sessions only consisted of fMRI-NFT. The fifth session began with fMRI-NFT, followed by an assessment of neural measures and a behavioral assessment. All neural assessments and fMRI-NFT procedures were performed inside the MRI scanner while the behavioral assessments were completed outside of the MRI.

2.3. Image data acquisition

All MRI procedures were conducted on a 3 T (T) MRI (Discovery 750 W, GE Healthcare, Madison, WI) using a 24-channel head coil. FMRI data

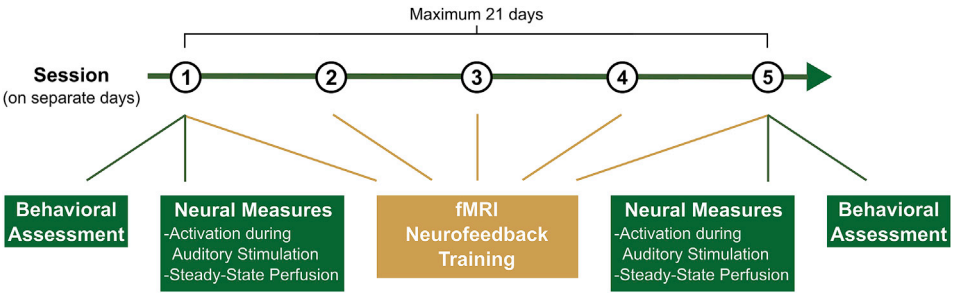

Fig. 1. Overview of the experimental design. The first session began with an initial assessment of behavior and neural measures followed by fMRI-NFT. The second, third, and fourth sessions consisted of only fMRI-NFT. The fifth session started with fMRI-NFT followed by a second assessment of neural measures and behavior.

(T2*-weighted) were collected using a gradient-recalled-echo (GRE) sequence sensitive to the BOLD signal. This sequence acquired data using the following parameters: 64 × 64 element matrix, 41 slices oriented parallel to the AC-PC plane, 3.5 × 3.5 × 3 mm^3 voxel size, 0.5 mm slice gap, 2000 ms repetition time (TR), 20 ms echo time (TE), a flip angle of 90°, and fat suppression was enabled. In previous unpublished data, these parameters were shown to reduce susceptibility artifacts which can be significant at high field strengths such as 3 T. TE was chosen to allow for high SNR in the cortex while minimizing the effects of susceptibility in deeper structures associated with attentional control, including the ventromedial prefrontal cortex (Fera et al., 2003; Hyde et al., 2001; Shinozaki et al., 2013; Wager et al., 2011).

Structural (T1-weighted) images were acquired using a 3D brain volume imaging (BRAVO) pulse sequence imploring an inversion recovery prepared fast spoiled gradient-echo (FSPGR). The structural images were acquired using a 256 × 256 element matrix, 172 slices oriented in the same plane as the functional scans, 1 mm^3 isotropic voxels, 0.8 phase field of view factor, inversion time (TI) = 450 ms, TE = 3.224 ms, a flip angle of 13°, and an auto-calibrated reconstruction for Cartesian sampling with a phase acceleration factor of 2.0.

Images of cerebral perfusion were acquired using a pseudo-continuous arterial spin labeling (pcASL) technique (Silva and Kim, 1999) with inversion (tagging) pulses administered immediately inferior to the imaging volume. All acquisitions used a post-label delay time (PLD) of 2025 ms. Five background suppression pulses were applied to reduce the signal of stationary tissues (Dixon et al., 1991; Mani et al., 1997; Ye et al., 2000) and improve signal-to-noise ratio (SNR) of arterial blood. A 3D fast spin echo (3D FSE) sequence was used for acquisition of the imaging volume. To reduce motion sensitivity, improve acquisition time, and minimize susceptibility artifacts, a stack-of-spirals readout gradient starting at the center of k-space was used (Glover, 2012). A total of 8 spiral arms were used for k-space sampling. Echoes were re-binned to Cartesian space in a 128 × 128 matrix, with TR = 4640 ms, TE = 10.7 ms, voxel size = 1.875 × 1.875 mm, slice thickness = 4 mm, and flip angle = 111°. The sequence acquired a total of 3 tag/control pairs with a total acquisition time of 4 min 46 s. During the scan, participants were instructed to remain awake and focus on a fixation dot presented on the display. This condition has demonstrated significantly greater reliability in resting-state functional MRI across all within-network connections, as well as within default-mode, attention, and auditory networks when compared to eyes open (no specified fixation) and closed methods (Patriat et al., 2013).

2.4. FMRI-NFT

Prior to entering the MRI environment, MRI screening forms were reviewed by a registered MRI technician. Female participants were required to take a urine dipstick pregnancy test. Once entering the MRI, the participants first inserted MRI-compatible ear plugs (MagnaCoil, Magnacoustics Inc., Atlantic Beach, NY) capable of providing communication and auditory stimulation (Genesis Ultra, Magnacoustics Inc., Atlantic Beach, NY). Next, the participants were positioned supine on the MRI table, their head was padded to restrict motion, and the upper part of the 24-channel head coil was attached. Using a laser, the nasion was landmarked relative to the MRI. The landmarked position was moved to the center of the MRI bore.

Once positioned, the fMRI-NFT procedures began (Fig. 2). Each fMRI-NFT session consisted of a single run of bilateral auditory stimulation which was used to individually and functionally localize the AC. This scan is referred to as the "functional localizer", followed by two runs of attempted self-regulation supplemented with neurofeedback from the AC (referred to as closed-loop endogenous neuromodulation). Between the functional localizer and the closed-loop endogenous neuromodulation runs, a structural MRI was acquired. During this time, the left and right AC were manually identified using anatomical markers and an activation map produced from the functional localizer. Once identified, a volume-of-interest (VOI) was selected to determine the voxels utilized to generate the subsequent neurofeedback.

2.4.1. Binaural auditory stimulation

To identify the AC, a single run of binaural auditory stimulation was executed in a boxcar design with six (6) repetitions of OFF and ON blocks. The auditory stimulus was 10 kHz lowpass filtered white noise (Gu et al., 2010) with a 6 dB rolloff and a 0.5 s fade-in (Audacity 2.1.3, www.audacity.org). Broadband noise was chosen to minimize variation in AC signal response across subjects who were controlled for overall hearing loss, but not for tonal-specific deficiencies. Although robust across patients, this approach may not be optimal for delineation of the AC as it has been shown that EPI sequence noise is similar to a complex tone embedded in broadband noise (Langers and van Dijk, 2011; Langers et al., 2014a). The duration of each block was 20 s, and the first block began after the acquisition of four (4) dummy volumes and one (1) software preparation volume. Binaural auditory stimulation was delivered via the headphones only during ON blocks and controlled via a stimulus presentation software (Presentation, Neurobehavioral Systems, Inc., Berkeley, CA). A continuous scan protocol was chosen to minimize differences between the AC localization procedure and subsequent NFT, although it has been shown that sparse scan designs can produce overall better localization of the AC (Langers et al., 2014b). The participants were not required to respond in any way during the scan, however they were instructed to remain awake and to focus on a round fixation dot presented in gray with a black background on a MRI-compatible display (SensaVue, Invivo, Gainesville, FL).

2.4.2. VOI selection

Immediately following acquisition, the BOLD data were pre-processed using custom MATLAB and C++ software. The pre-processing included standard spatial filtering (3D, 5-point Gaussian low-pass kernel, full-width half-maximum of 7 mm), motion correction (corrected to the first volume using a rigid-body 3-parameter model) and temporal filtering (5-point Gaussian low-pass kernel, sigma of 3 s) processing functions (Friston et al., 1995).

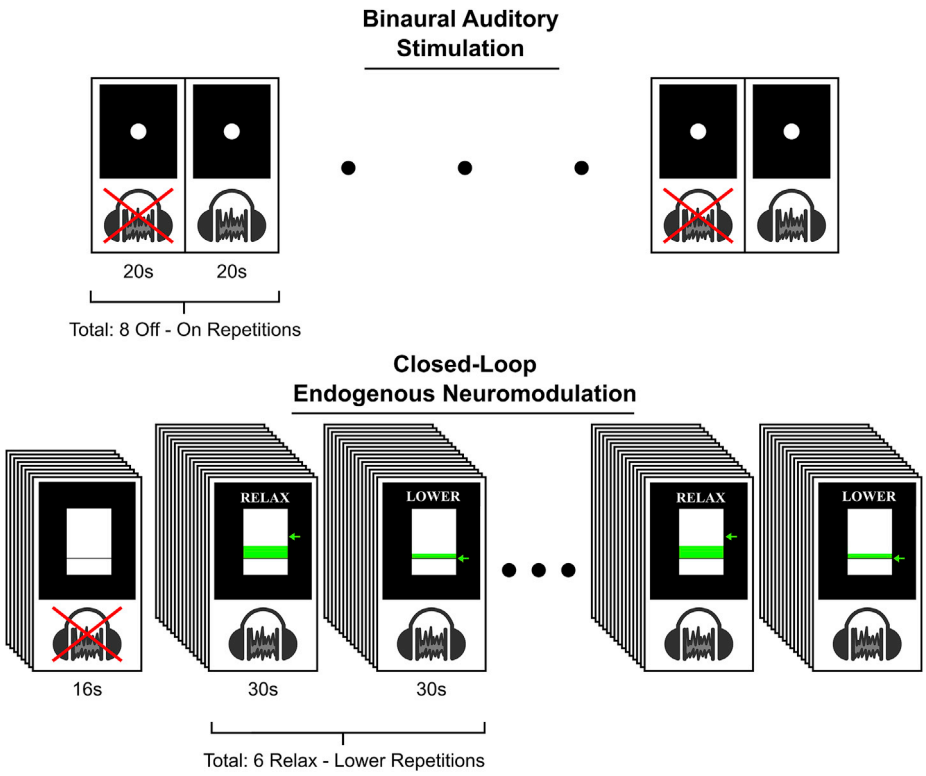

Fig. 2. Overview of each fMRI-NFT session. Each session began by acquiring BOLD data during a blocked binaural auditory stimulation paradigm. Next, a volume-of-interest for subsequent neurofeedback was selected from activated voxels in the right and left AC. Finally, two runs of closed-loop endogenous neuromodulation were executed to train AC down-regulation.

An activation map was created by defining a single explanatory variable (EV) by convolving a boxcar model containing 20 s control and task conditions with a pre-defined HRF (Ashby, 2011). Next, the BOLD data at each voxel was fit to the model using a general linear model (GLM) by applying a weight of +1 to the EV, representative of activation (positive correlation to the model). The resulting β parameter maps were converted to t statistic maps (activation maps) using standard statistical transforms. The region in the AC in which the feedback signal for the subsequent closed-loop endogenous neuromodulation runs was derived from this activation map. Voxels were added to the auditory VOI by first locating the axial slice in which the inferior surface of the anterior ventricle horns are visible. Then, activation patterns on the left and right hemispheres near the posterior end of the lateral sulci were observed in this slice and the slices immediately inferior and superior to the slice containing the inferior surface of the anterior ventricle horns. The *t* statistic threshold was adjusted to reveal approximately 10–15 connected voxels per hemisphere across these three slices. Voxels surviving this threshold and located within these regions were added to the VOI to complete the determination of the functional localizer.

2.4.3. *Closed-loop endogenous neuromodulation*

Following the functional localizer, two runs of closed-loop endogenous neuromodulation were completed. Four dummy volumes and one software preparation volume were acquired first. Then, eight volumes were acquired to determine a baseline BOLD signal value for the selected auditory VOI. During the acquisition of the baseline volumes, a countdown was displayed on the screen beginning at 16 s; however, there was no auditory stimulation during either the eight baseline volumes or the four preparatory volumes.

After baseline, six repetitions of 30 s relax and lower blocks were completed in a boxcar-design. Both blocks were accompanied with binaural auditory stimulation using the same continuous noise from the functional localizer. During relax, every participant was instructed to relax and clear their mind, resulting in an increase in the feedback signal. They were also instructed to keep their eyes open. Participants were instructed to lower the feedback signal during lower blocks by performing a mindfulness task wherein they should decrease brain activity associated with auditory input. A list of four example mindfulness tasks were provided, giving the participants a few starting points.

During these relax and lower plots, a feedback signal was computed and displayed to the EXP participants from real-time analyses of BOLD data. These real-time analyses were implemented in custom MATLAB and C++ software and included standard spatial filtering (3D, 5-point Gaussian low-pass kernel, full-width half-maximum of 7 mm) and motion-correction (corrected to the first volume of the functional localizer using a rigid-body 3-parameter model) processing functions (Friston et al., 1995). This custom software further compared the average BOLD signal in the auditory VOI during the 8 baseline volumes to that of the current volume to derive a percent signal change. The current feedback signal was determined by temporally-filtering (5-point Gaussian low-pass kernel consisting of only past components, sigma of 3 s) the percent BOLD signal change with the feedback signals from previous volumes.

This feedback signal was presented to the participants using a thermometer-style bar plot where the height of the bar was proportional to the percent signal change from baseline. A change of 1% in the BOLD signal resulted in a bar height of 1° visual angle. Furthermore, an arrow appeared to the right of the bar plot to act as a target line for the feedback bar. During relax blocks, the arrow was placed at a height equivalent to 1% as the auditory VOI BOLD signal should increase relative to baseline due to the auditory stimulation. In the lower blocks, the arrow appeared at a height equivalent to 0% tasking the participants with lowering the auditory VOI response to the auditory stimulation to the level when no stimulation is provided. Task instructions (*i.e.,* relax and lower) indicating the current block were additionalluy supplied above the thermometer plot. For participants in the control group, the feedback display and instructions were equivalent to the EXP group but the feedback

signal used to determine the height of the feedback bar was yoked from a random EXP participant but matched for experimental progress. Both runs from each session were duplicated from the same EXP participant but the EXP participant was selected randomly each session. The goal of the feedback was for participants to learned mindfulness tasks that are most successful in regulating the auditory cortex.

2.5. Behavioral assessment

Behavioral measures of attentional control were collected using one questionnaire and two computerized tasks. These tasks were conducted using a laptop outside of the MRI. The participants wore active noise-cancelling headphones (Samsung Level, Samsung Electronics America, Ridgefield Park, NJ) to mitigate distracting sounds during the tasks. The questionnaire provided subjective measures of attentional control while the computerized tasks provided objective measures. The attentional control scale (ACS; Derryberry and Reed, 2002) was completed using digitized version (Qualtrics, Provo, UT) to measure the general capacity for attentional control. Sub-factors of the ACS include measures of the ability to focus attention, shift attention between tasks, and flexibly control thought.

The attention to emotion task (AE; Harris and Pashler, 2004; Moray, 1959) requires participants to make a speedy judgement about the parity of two digits separated by a word. In a limited number of scattered trials, response times are significantly slowed when the word is the participant's own name evaluating the impact of emotion of attention. Harris and Pashler (2004) found that when a person's name or an emotionally charged stimulus is presented, the stimulus may or may not be enough to warrant recognition likely subject to the attentional capacity limitations found in similar tasks utilizing more "ordinary" stimuli. We implemented this task to determine the influence of, if any, fMRI-NFT on attentional control. The AE task was controlled via a stimulus presentation software (Presentation, Neurobehavioral Systems, Inc., Berkeley, CA). One hundred and thirty trials were executed, each beginning with a gray fixation point presented for 500 ms. The stimuli followed the fixation and consisted of two digits (1–9) in gray flanking a word presented in green. The stimuli were presented for 150 ms. Neutral (*i.e.*, ordinary) words appeared in 100 trials and 30 trials contained the participant's name (*i.e.,* emotionally-charged stimulus). No neutral words were repeated within a single session. After the stimulus, there was a feedback period with a duration dependent upon the response time. The feedback period was limited to a minimum of 500 ms and maximum of 5000 ms. Participants were to use this time to indicate whether the digits were both even or odd (left control button) or mismatched (right control button). Half of the name and half of the neutral trials mismatched, the other half matched. The trials were randomized apart from the first fifteen trials which contained only neutral trials. Finally, a 1000 ms inter-trial interval (ITI) separated the start of the next trial and the preceding response.

The continuous performance test (CPT) was developed to measure deficits in sustained attention (Chen et al., 1998). A variant of the CPT was developed as a simultaneous discrimination and vigilance task (CPT-X). The CPT-X uses a single character or number as a target and a response is inhibited when the stimulus matches the target. This task was implemented to measure sustained attention and vigilance. The CPT-X contained 300 trials separated evenly across four continuous blocks controlled via the stimulus presentation software. Each block contained 15 matching trials and 60 non-matching trials. The order of the stimuli was randomized within each block. The stimuli consisted of capitalized letters from the English alphabet with 'X' being the target. Participants were instructed to press the right control button when the stimulus did not match the target and inhibit this response when the stimulus matched the target. The stimulus was presented for 500 ms in gray upon a black background. An ITI randomly sampled from 500, 700, and 900 ms separated each stimulus to prevent participants from predicting the presentation of stimuli. During this period, a gray fixation point was presented on a black background.

2.6. Neural assessment

The single run of binaural auditory stimulation was utilized to assess changes in the neural auditory response. This was executed during prior to closed-loop endogenous neuromodulation as part of fMRI-NFT but was also repeated after fMRI-NFT on the fifth session. Additionally, a baseline measure of steady-state perfusion was acquired during the first session prior to fMRI-NFT. A second measure of steady-state perfusion was collected during the last session following fMRI-NFT. During this scan, participants were instructed to remain awake and to focus on the focal point displayed on the screen.

2.7. Data analysis

2.7.1. Closed-loop endogenous neuromodulation

The BOLD data acquired from each closed-loop endogenous neuromodulation run was processed using the FMRIB Software Library (FSL; Smith et al., 2004; Woolrich et al., 2009). First, individual (first-level) analyses were conducted on each of the 4D fMRI data sets. Prior to the individual analyses, pre-processing was performed using standard techniques. These consisted of applying a high-pass temporal filter (Gaussian-weighted least-squares straight line fitting, cut-off = 60 s) to each voxel, correcting for motion by registering each volume to the center volume of the data set (rigid-body 12-parameter model; Jenkinson et al., 2002), creating a brain mask from the first volume and applying to each subsequent volume (Smith, 2002), spatial filtering on each volume using Gaussian convolution (full-width half-maximum of 5.625 mm), and removing low-frequency trends using a local fit of a straight line across time at each voxel with Gaussian weighting within the line to create a smooth response.

Next, individual analyses were conducted on each of the 4D fMRI data sets. A single EV was defined by convolving a boxcar model containing 30 s rest and task conditions with a hemodynamic response function (HRF; modeled by a gamma function; phase offset = 0 s, standard deviation = 3 s, mean lag = 6 s). The temporal derivative of the original waveform was added to the result and the temporal filter used in pre-processing was applied. The data set was fit to the model using a general linear model (GLM) with prewhitening by applying a weight of −1 to the EV, representative of de-activation during closed-loop endogenous neuromodulation (negative correlation with the model). Z statistic maps were created using standard statistical transforms to convert the β parameter maps. A clustering method allowed us to account for false positives due to multiple comparisons. This method considers adjacent voxels with a z statistic of 2.3 or greater to be a cluster. The significance for each cluster was estimated and compared to a threshold of $p < 0.05$ using Gaussian Random Field theory. The significance of voxels that either did not pass the significance level threshold or do not belong to a cluster were set to zero. A mean image of the data set was registered to the individual's high-resolution structural image by estimating motion from a boundary-based registration method including a fieldmap-based distortion correction (Greve and Fischl, 2009), then further registered to the MNI-152 T1-weighted 2 mm template provided in FSL (Collins et al., 1995; Mazziotta et al., 2001) using a 12-parameter model (Jenkinson et al., 2002; Jenkinson and Smith, 2001). The z statistic maps were converted to standard space using the transform responsible for morphing the mean image of each data set to the template to co-register all volumes.

Next, we performed a VOI analysis to determine each participants ability to down-regulate the auditory cortex. We converted the target VOI coordinates from each fMRI-NFT session to a binary mask. Since the VOI was determined from the first volume of the functional localizer, motion was corrected in the functional localizer data by registering each volume to the first volume using the method described above and creating a mean image. Next, the mean image of each neuromodulation run was registered to the mean image of the associated functional localizer using a rigid-body 12-parameter model. The transform responsible for

morphing the mean image of each neuromodulation run was applied to the associated VOI mask. AC down-regulation was assessed in both groups by masking the cluster-corrected de-activation map from above with the registered VOI mask. A 2×2 (between-subjects factor: group; within-subjects factors: session and run) repeated measures ANOVA was performed on AC down-regulation using SPSS (IBM SPSS statistics version 24.0, IBM Corp., Amonk, New York) to compare the overall change in volitional control from session 1 run 1 to session 5 run 5.

Finally, we performed a voxel-based group (second level) analysis using the results of the first level. A 2×2 (between subject factor: group; within-subjects factor: session) repeated measures ANOVA was implemented in FSL with a mixed-effects method. Runs 1 and 2 from the first and last fMRI-NFT session were included to assess the overall changes associated with learning down-regulation of the AC. Prior to running this analysis, each individual de-activation map was masked to remove activated voxels. This enabled us only to assess changes in de-activation as the results of the ANOVA are bi-directional. The ANOVA analysis assumed the covariance between measures within-subject follow a compound symmetric structure (equal variance and intra-subject correlations being equal). This assumption is valid as the data was acquired in close proximity and regularly sampled. Two contrasts were created to identify voxels with stronger de-activation during the fifth training session than the first session and a larger change in de-activation from the first to fifth training session (5–1) for the EXP group when compared to the CON group. *Z* statistic maps, created by transforming the resulting β parameter maps using standard statistical transforms, were thresholded using the clustering method outlined above with a *z* statistic threshold of 1.96. Furthermore, β parameter estimates from each of these contrasts underwent separate *F* tests to explore the main effect of session and the session by group interaction. This analysis lacked the degrees of freedom necessary to include the main effect of group and, therefore, this contrast was not included. *Z* statistic images were created from *F* statistic images using standard statistical transformations.

2.7.2. Behavioral assessment

The ACS total score was computed for each participant/session by summing the scores from the responses. A 2×2 repeated measures ANOVA (between-subjects factor: group; within-subjects factor: session) was completed in SPSS on the ACS total score to assess changes across pre- and post-training assessments. *Post hoc*, Bonferroni-corrected pairwise comparisons were conducted on significant interaction effects.

The AE was analyzed to measure latency (*i.e.,* response time) to determine the effect of emotionally-charged stimuli on response time as a measure of distractibility and attentional control whereas if emotionally-charged stimuli should increase the response time (*i.e.,* distract) then attentional control is lower. Each trial was categorized as correct or incorrect. Mean latency was determined for the correct responses from each type (emotional or neutral) and session. A test statistic to analyze for outliers was performed using the following equation:

$$T1 = \frac{\mathrm{x(n)} - \mathrm{x}}{s} \tag{1}$$

where ***x(n)*** is the latency of a single observation, *x* is the mean latency, and *s* is the standard deviation. The test statistic was compared to a critical value of 3.27 (Lovie, 1986). A final mean latency was recalculated by using the latencies with test statistics less than the critical value. To determine a measure inversely related to attentional control, the difference between the mean emotional and neutral latencies were computed as a percent change (ΔAE mean latency).

Assessment of the CPT-X was founded upon signal detection theory (SDT; Green and Swets, 1966). Each trial was separated into one of four possibilities according to SDT: 1) target was not present and the response was indicated (*i.e.,* correct rejection), 2) target was present and the response was inhibited (*i.e.,* hit), 3) target was not present and the response was inhibited (*i.e.,* false alarm), and 4) target was present and the response was indicated (*i.e.,* miss). Using the hit and false alarm rates from each session, an index of sensitivity (d', *i.e.,* discriminability) was computed using the procedures previously verified (Sorkin, 1999). Sensitivity is desirable as it is free from motivational effects (Swets and Sewall, 1963). In summation, this process finds the *z* scores for which the standard normal cumulative distribution equals the hit and false alarm rates. The *z* score for the false alarm rate became indeterminate when the no false alarms were made, which was the case in several sessions. Therefore, a corrected false alarm rate was calculated when no false alarms were present using the equation:

$$1 - 2^{-1/t} \tag{2}$$

where *t* is the number of correct rejection trials. Then, d' is calculated as the difference between the *z* score for the hit and false alarm rate ($z_{\mathrm{hit}} - z_{\mathrm{false\_alarm}}$).

2×2 repeated measures ANOVAs similar to that described for ACS total score were also completed on ΔAE mean latency and CPT-X sensitivity separately to assess changes across pre- and post-training assessments. *Post hoc*, Bonferroni-corrected pairwise comparisons were conducted on significant interaction effects. The ANOVAs were all completed using SPSS. In the ANOVAs, Mauchly's Test of Sphericity could not be conducted on the within-subjects factors because there were only single differences to compute between factor levels and, therefore, no comparison to be made so sphericity was assumed.

2.7.3. Binaural auditory stimulation

The BOLD data from the session 1 pre-NFT and session 5 post-NFT binaural auditory stimulation runs underwent similar processing as the closed-loop endogenous neuromodulation runs. The pre-processing was the same with the exception of the high-pass temporal filter which used a cut-off of 40 s. After pre-processing, a single EV was defined by convolving a boxcar model containing 20 s rest and task conditions with the HRF. The temporal derivative of the original waveform was added to the result and the temporal filter described above was applied to the model. The data were fit to the model using a GLM with prewhitening by applying a weight of +1 to the EV, representative of activation during the task (positive correlation with the model). *Z* statistic maps were created using standard statistical transforms to convert the *β* parameter maps. The clustering method outline above was implemented with a *z* statistic threshold of 2.3. A mean image of the data was registered to the individual's high-resolution structural image by estimating motion from a boundary-based registration method including a fieldmap-based distortion correction, then further registered to the MNI-152 T1-weighted 2 mm template provided in FSL using a 12-parameter model. The *z* statistic maps were then converted to standard space using the transform responsible for morphing the mean image of each data set to the template to co-register all volumes.

Group (second level) analyses were performed in FSL using to conduct 2×2 (between subject factor: group; within-subjects factor: session) repeated measures ANOVAs on a voxel-by-voxel basis in FSL with a mixed-effects method. Again, the data was acquired close in proximity and regularly samples, validating the assumption of compound symmetry. Two contrasts were created to identify voxels more active during the session 5 post-NFT than session 1 pre-NFT and a larger change in activation between these runs for the EXP group than the CON group. *Z* statistic maps, created by transforming the resulting *β* parameter maps using standard statistical transforms, were thresholded using the clustering method outlined above with a *z* statistic threshold of 1.96. Furthermore, *β* parameter estimates from each of these contrasts underwent separate *F* tests to explore the main effect of session and the session by group interaction. This analysis lacked the degrees of freedom necessary to include the main effect of group, therefore this effect was not included. *Z* statistic images were created from *F* statistic images using standard statistical transformations.

2.7.4. Steady-state perfusion

Steady-state perfusion was assessed from ASL to quantify CBF, measured in units of mL/100 mg/min. Calculation of CBF maps was performed using automated functions in the GE reconstruction software. First, the 3 tagged and 3 control volumes were first averaged in place (without motion correction). Then, difference images were calculated for all patients by subtracting the average tagged volume from the average control volume automatically. Finally, quantitative CBF maps were generated from the difference images, the proton density (PD) weighted volumes, and a standard single compartment model (Alsop et al., 2015; Alsop and Detre, 1996; Mutsaerts et al., 2014). Data from two (2) participants (1 CON, 1 EXP) were corrupted, thus the analysis includes the remaining 8 CON and 17 EXP participants.

The CBF maps from each day and session run were processed using the FSL on a 74-core Rocks Cluster Distribution (www.rocksclusters.org) high-performance computing system capable of running 120 threads in parallel. First, individual (first-level) analyses were conducted on each of the CBF maps. The PD-weighted images acquired were registered to the individual's high-resolution structural image by estimating motion from a boundary-based registration method including a fieldmap-based distortion correction, then further registered to the MNI-152 T1-weighted 2 mm template provided in FSL using a 12-parameter model. The CBF maps were converted to standard space using the transform responsible for morphing the PD-weighted image of each data set to the template in order to co-register all volumes.

Next, group non-parametric statistical analyses were performed on the session 1 pre-NFT and session 5 post-NFT co-registered CBF maps using permutation testing implemented using FSL randomise (Anderson and Robinson, 2001; Winkler et al., 2014). Due to our mixed-model design, we were not able to perform an analysis of variance (ANOVA) using this approach. Instead, two separate analyses were performed. In the first approach, an analysis was conducted across training combining the two groups to evaluate the effect of session. Null *t* distributions for contrasts representative of the main effect of session were derived by performing 1,000,000 random permutations (Nichols and Holmes, 2003). A clustering method described in the group analysis above allowed us to account to false positives due to multiple comparisons.

The interaction of group and session was assessed using a single unpaired approach. The change in CBF between the session 1 pre-NT and session 5 post-NFT co-registered CBF maps were calculated for each subject. Next, the statistical significance of the group differences in the change in CBF was determined using permutation testing implemented using FSL randomise. Null *t* distributions for contrasts representative of the interaction of session and group were derived by performing 1,000,000 random permutations and the clustering method outlined above was implemented to account for false positives.

3. Results

3.1. Hearing thresholds

Hearing thresholds were compared across groups for each frequency tested (250 Hz, 500 Hz, 1 kHz, 2 kHz, 3 kHz, 4 kHz, and 6 kHz) using Welch's *t*-test (Fig. 3). To be most conservative in the detection of a potential group difference, no correction for multiple comparisons was applied. There were no observed significant differences ($p > 0.05$, two-tailed) for any of the testing frequencies signifying the two groups had equivalent hearing thresholds between 250 Hz and 6 kHz. It is important to note, the transducers utilized in this test were calibrated but were not noise-attenuating. Therefore, the measured hearing levels may appear greater in testing frequencies less than 2 kHz due to ambient noise (*e.g.*, HVAC noise) transversing the ear cups especially since a soundproof room was not utilized for testing.

3.2. AC control

A 2×5 repeated measures ANOVA evaluated the size of the functionally-defined AC VOI across sessions and groups (Fig. 4). The size of the VOIs did not significantly differ between groups or sessions ($F_{1,100} = 0.208$, $p = 0.208$ and $F_{4,100} = 0.740$, $p = 0.567$, respectively, two-tailed). Furthermore, the interaction of session by group was not significant in the VOI size ($F_{4,100} = 0.531$, $p = 0.713$, two-tailed). Although the VOIs for the CON group were not used during neurofeedback, these VOIs were utilized for post-processing to compute AC de-

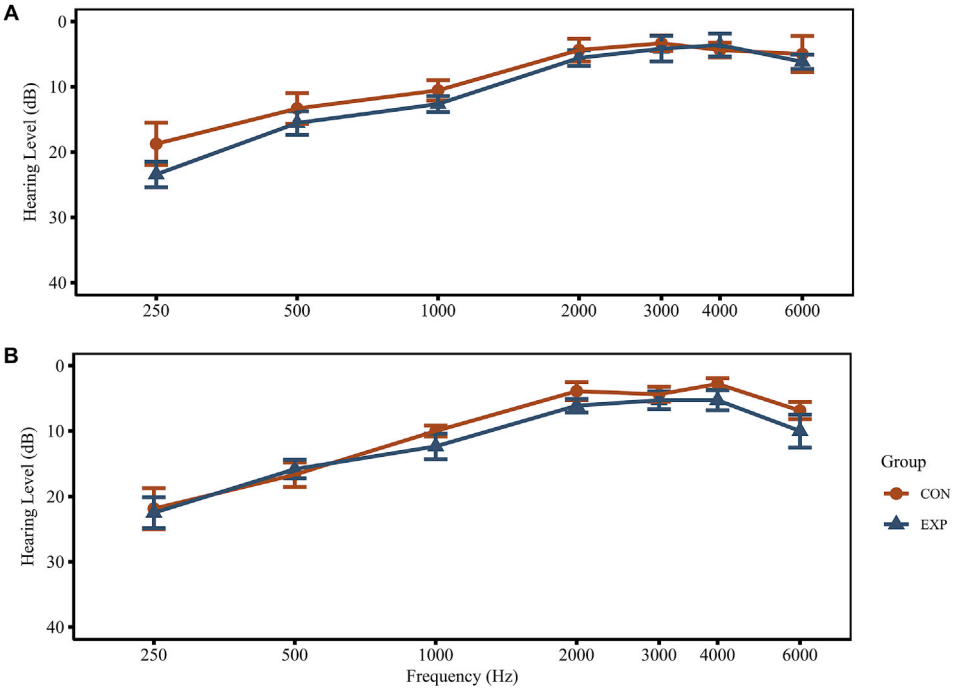

Fig. 3. Audiogram results for the hearing levels of the (A) left and (B) right ear separated by group and frequency. No significant differences were observed between groups for all testing frequencies.

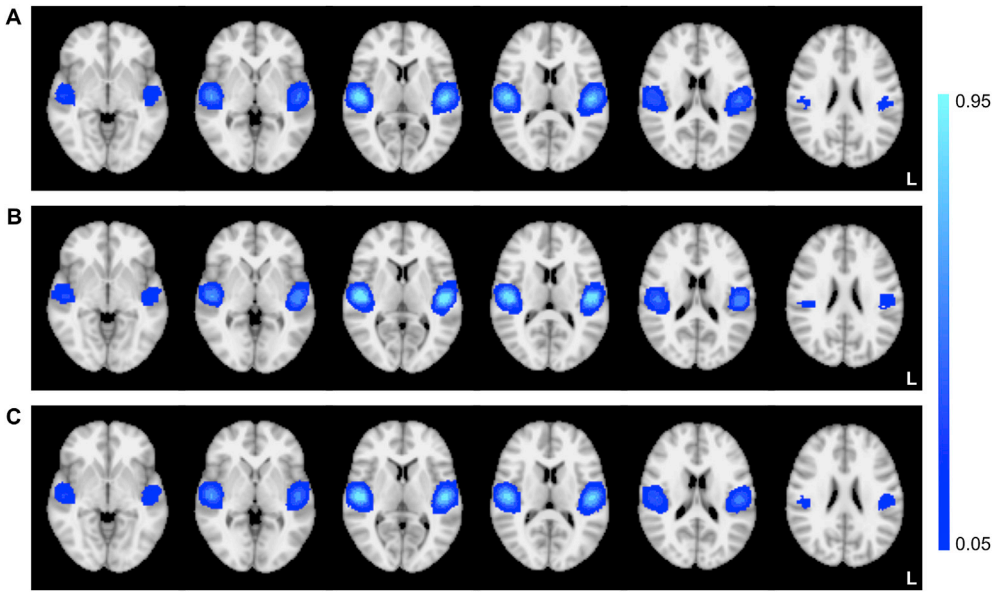

Fig. 4. The probability of voxel inclusion during fMRI-NFT for (A) both EXP and CON groups, (B) EXP group only, (C) CON group only. VOIs were transformed to standard space using the same transformation responsible for morphing the fMRI data to standard space. Axial slices are displayed at MNI coordinates z = −6, 0, 8, 12, 18, and 24 mm (left to right).

activation. The average size of each VOI across groups and sessions was 1490 $mm^3 \pm 283.15\ mm^3$.

A 5 × 2 × 2 repeated measures ANOVA evaluated the effects of session, run, and group on AC de-activation during closed-loop neuromodulation (Fig. 5A). AC de-activation is representative of an individual's ability to volitionally down-regulate the AC (*i.e.,* AC control). The results of the between-subjects effect revealed a significant main effect of group ($F_{1,25} = 3.941$, $p = 0.029$, one-tailed). One-tailed statistics are reported as the *a priori* hypothesis was that AC control would be greater in the EXP group. Maulchly's test of sphericity was not significant for session ($p = 0.160$, two-tailed) or session by run interaction ($p = 0.776$, two-tailed). These results validate the assumption of sphericity, which was used to assess the results of the within-subjects tests henceforth. The results of the within-subjects testing identified a significant main effect of session ($F_{4,100} = 2.702$, $p = 0.0175$, one-tailed). One-tailed statistics are reported as our *a priori* hypothesis was that AC control would increase with training. The main effect of run was not significant ($F_{1,25} = 0.338$, 0.283, one-tailed) along with the interaction effects of session by group ($F_{4,100} = 0.930$, $p = 0.225$, one-tailed), run by group ($F_{1,25} = 0.908$, $p = 0.175$, one-tailed), session by run ($F_{4,100} = 1.772$, $p = 0.07$, one-tailed), and session by run by group ($F_{4,100} = 0.953$, $p = 0.219$, one-tailed). *Post hoc*, Bonferroni-corrected pairwise comparisons were conducted on the session by group interaction to evaluate differences between sessions 2, 3, 4, and 5 with session 1.

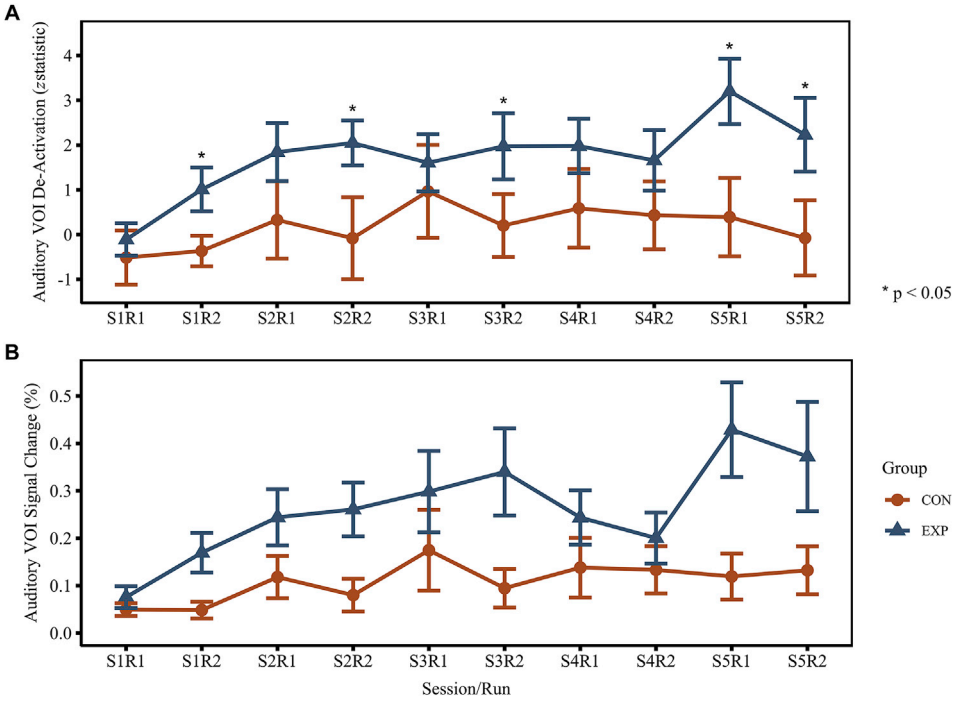

Fig. 5. Results from the AC VOI across all sessions and runs. VOI de-activation (A) and signal change (B) separated by group, session, and run.

These results revealed there were significant differences between sessions 5 ($p = 0.006$, one-tailed) and 2 ($p = 0.015$, one-tailed) in the EXP group while the remaining two sessions (2 and 3) were close to significant ($p = 0.0528$ and $p = 0.0502$, respectively). For the CON group, no comparison was near significant ($p > 0.4$ for all comparisons). Welch's *t*-test were conducted between the groups for each session/run. The EXP group had significantly greater AC control than the CON group for session 1 run 2 ($p = 0.015$, one-tailed), session 2 run 2 ($p = 0.0385$, one-tailed), session 3 run 2 ($p = 0.048$, one-tailed), session 5 run 1 ($p = 0.012$, one-tailed), and session 5 run 2 ($p = 0.0315$, one-tailed). For reference, the percent signal changes in the auditory VOI (Fig. 5B) are presented along with the auditory VOI de-activation values.

A voxel-based 2×2 (group by session) repeated measures ANOVA was performed using FSL. The *F* test revealed a significant ($z > 1.96$) main effect of session on de-activation magnitude during neurofeedback in several regions throughout the brain, including bilateral changes in AC (Fig. 6). It is important to note that we cannot identify which regions had stronger de-activation during neurofeedback in the fifth session than the first due to the bi-directionality of the *F* test. The contrasts identifying voxels with significantly greater activation and de-activation in session 5 than session 1 were assessed to clarify the directionality. We observed all of these regions in the de-activation contrast, implying directionality towards stronger de-activation in the fifth neurofeedback session, which supports the results of the VOI analysis.

Additionally, the *F* test revealed a significant ($z > 1.96$) interaction of session by group on de-activation during neurofeedback (Fig. 7). Bilateral changes were found in the thalamus, lingual gyrus, and the cuneus. Changes in the superior frontal gyrus, medial frontal gyrus, inferior frontal gyrus, precentral gyrus, and postcentral gyrus only appeared in the left hemisphere. In *post hoc* comparisons, a few small regions were significantly more de-activated in the EXP group than the CON group during session 1 with local maxima appearing in the right middle frontal gyrus and the left fusiform (Fig. 8A). The bilateral auditory cortex appeared in the contrast identifying voxels significantly more de-activated in the EXP group at session 5, along with local maxima in the right inferior frontal cortex, right middle frontal gyrus, and the left middle temporal gyrus (Fig. 8B). There were significant differences in de-activation between sessions 1 and 5 for the CON group in the auditory cortex as well as local maxima in the left middle frontal gyrus, bilateral superior frontal gyrus, and left inferior parietal lobule (Fig. 9A). The EXP group also shows significant differences in de-activation from session 1 to session 5 as the CON group, but to a larger magnitude and extent (Fig. 9B).

3.3. Behavioral assessment

The effects of group and session on ACS total score, a subjective measure of attentional control, were evaluated using a repeated-measures ANOVA. The between-subjects effects revealed the main effect of group was not significant ($F_{1,25} = 0.029$, $p > 0.05$, one-tailed). The results of the within-subjects testing identified the main effect of session was not significant ($F_{1,25} = 0.01$, $p > 0.05$, one-tailed). The interaction effect of session and group was not significant ($F_{1,25} = 0.104$, $p > 0.05$), therefore no *post hoc* testing was performed.

A repeated measures ANOVA evaluated the effects of group and session on ΔAE mean latency. The results of the tests of between-subjects effects revealed the main effect of group was significant ($F_{1,25} = 3.267$, $p = 0.042$, one-tailed), with a greater distractibility in the EXP group on average. The within-subjects testing identified the main effect of session and the session by group interaction effect were not significant ($F_{1,25} = 0.125$, $p = 0.364$ and $F_{1,25} = 0.012$, $p = 0.457$, respectively).

The results of the 2×2 repeated measures ANOVA for CPT-X sensitivity (d') revealed the main effect of group was not significant ($F_{1,25} = 0.507$, $p = 0.242$, one-tailed). The results of the within-subjects testing identified the main effect of session and the session by group interaction were not significant ($F_{1,25} = 1.095$, $p = 0.153$ and $F_{1,25} = 0.010$, $p = 0.461$, respectively). One-tailed statistics are reported as our *a priori* hypothesis was that ACS total score and CPT-X sensitivity would increase with training and ΔAE mean latency would decrease with training, and these changes would be greater in the EXP group.

3.4. AC control – behavior correlation

Changes across training in behavior (session 5 minus session 1) and AC control (session 5, run 2 minus session 1 run 1) were computed. Bivariate correlations (Table 1) were carried out in SPSS to evaluate the relationship between these changes in behavior and AC control under the hypothesis that those individuals with the greatest change in AC control will have more profound changes in behavior. The change in AC control was found to have a significant negative correlation with the change in ΔAE mean latency (Fig. 10; Pearson's $r = -0.323$, $p = 0.05$). Separated by group, the correlation was not significant for either the CON group (Pearson's $r = -0.183$, $p = 0.318$) or the EXP group (Pearson's $r = -0.347$, $p = 0.079$). The change in ACS total score and CPT-X sensitivity were not significantly correlated to AC control in neither combined nor group-separated analyses.

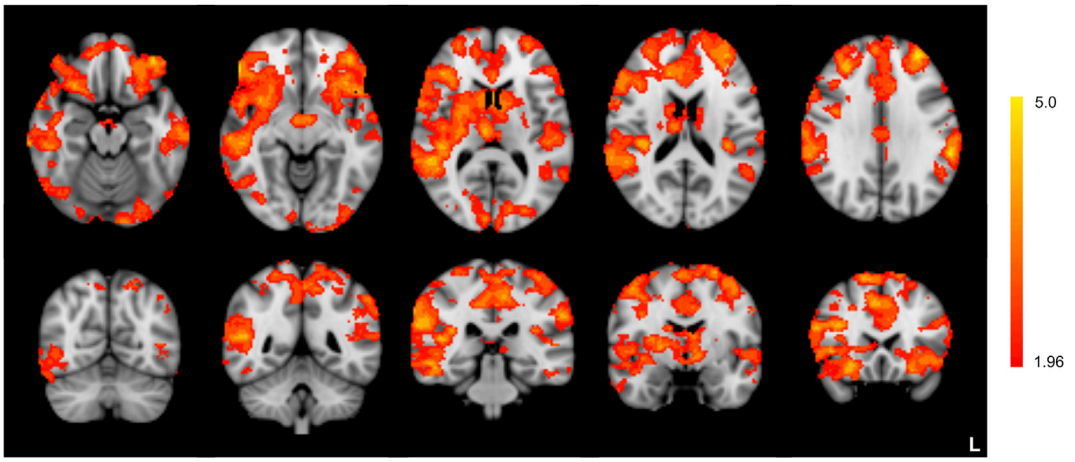

Fig. 6. *F* test results for the main effect of session indicate increased de-activation during neurofeedback across training for several brain regions. Axial slices (top row) are displayed at MNI coordinates $z = -18, -8, 10, 18$, and 30 mm (left to right). Coronal slices (bottom row) are displayed at MNI coordinates $y = -64, -48, -32, -4$, and 20 mm (left to right).

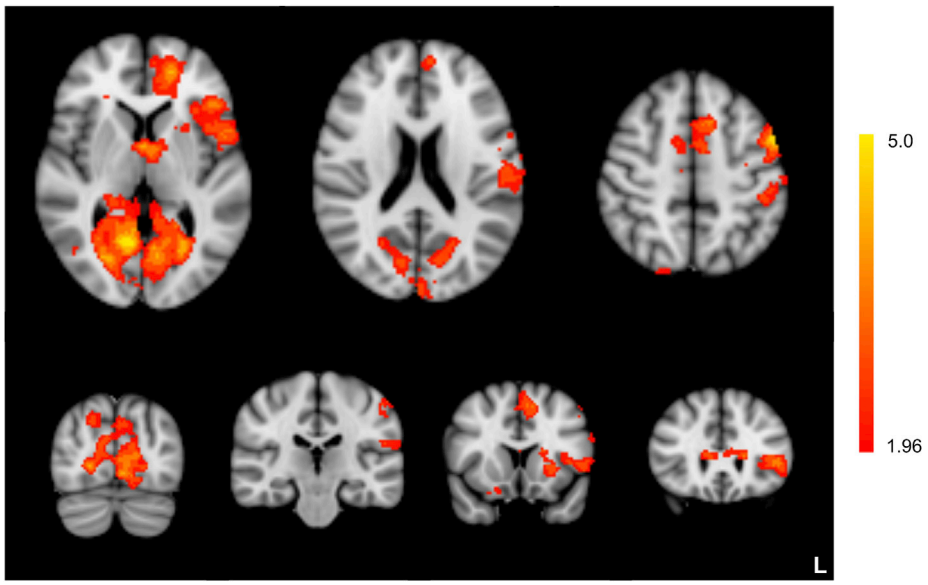

Fig. 7. *F* test results for the interaction of session by group from closed-loop endogenous neuromodulation. Axial slices (top row) are displayed at MNI coordinates z = 4, 20, and 50 mm (left to right). Coronal slices (bottom row) are displayed at MNI coordinates y = −76, −24, 14, and 26 mm (left to right).

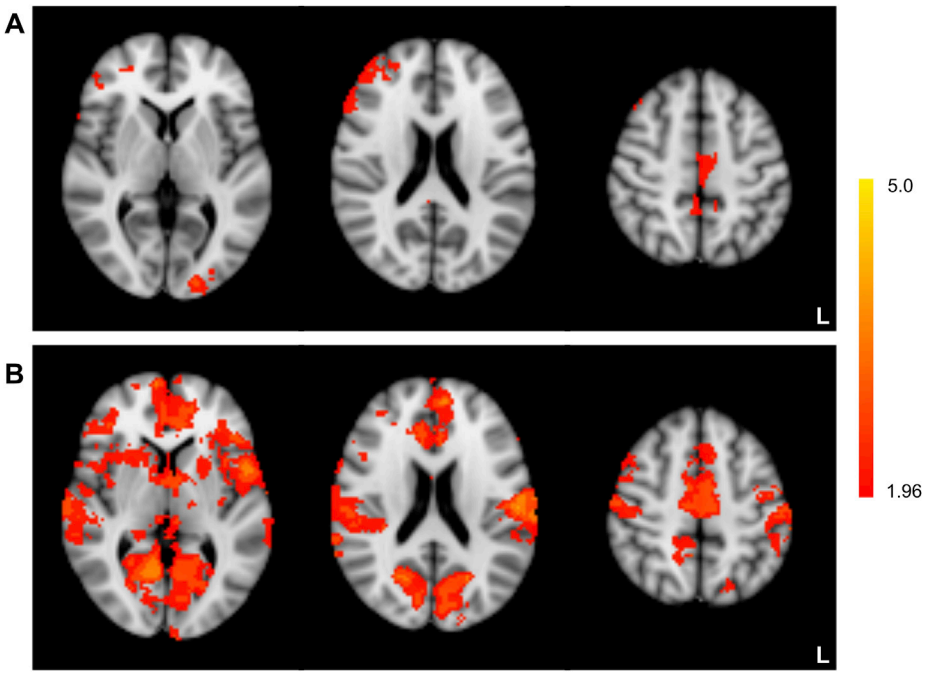

Fig. 8. Contrast identifying increased de-activation in the EXP group compared to the CON group during closed-loop endogenous neuromodulation for sessions 1 (A) and 5 (B). Axial slices are displayed at MNI coordinates z = 4, 20, and 50 mm (left to right).

3.5. Binaural auditory stimulation

A 2 × 2 (group by session) repeated measures ANOVA was performed using FSL. The *F* test revealed a significant ($z > 1.96$) main effect of session on activation magnitude during binaural auditory stimulation bilaterally in the precentral and postcentral gyri (Fig. 11). It is important to note that we cannot identify which regions had stronger activation or de-activation due to the bi-directionality of the *F* test, and whether this increased or decreased from session 1 to session 5. The contrasts identifying voxels with significantly greater activation and de-activation in session 5 than session 1 were assessed separately to clarify the directionality. We observed both the precentral and postcentral gyrus in the activation contrast, implying directionality towards stronger activation in the fifth session (Fig. 12A). The contrast identifying voxels less activated on session 5 than session 1 (or greater de-activation) revealed a significant effect in the right inferior frontal gyrus and bilateral auditory cortex (Fig. 12B). The *F* test did not reveal any significant findings for the interaction of session by group on activation during binaural auditory stimulation.

3.6. Steady-state perfusion

Permutation testing was conducted to evaluate the main effect of session and the interaction between session and group using two-sample paired and unpaired testing, respectively. A main effect of session was found in a few small clusters and are most likely false positives. The

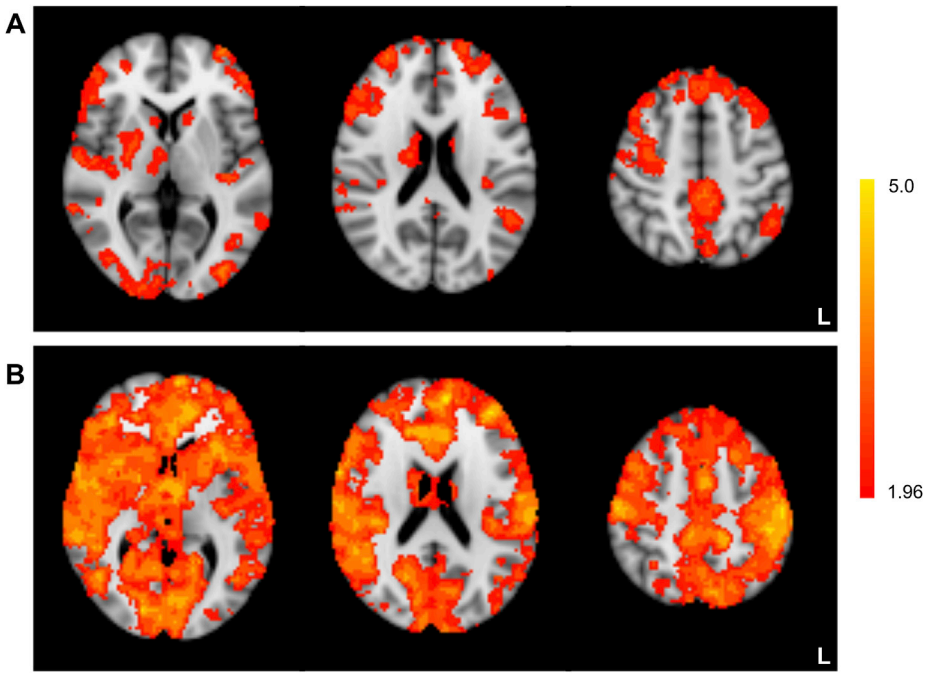

Fig. 9. Contrast identifying increased de-activation from session 1 to session 5 during closed-loop endogenous neuromodulation in the CON (A) and EXP (B) groups. Axial slices are displayed at MNI coordinates z = 4, 20, and 50 mm (left to right).

Table 1
Results of the bivariate correlation analysis. Highlighted columns indicate significance at or below p = 0.05.

		ACS Total Score	CPT-X Sensitivity (d')	ΔAE Mean Latency (%)
AC control	Pearson's r	.244	.119	-.323
	Significance (one-tailed)	.110	.277	.050
	n	27	27	27

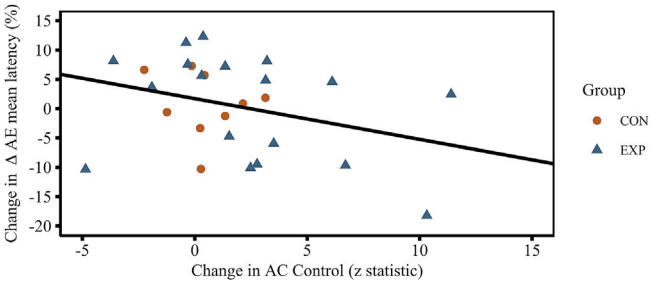

Fig. 10. Bivariate correlation results. A significant negative relationship (r = −0.323, p = 0.05) between the change in AC control and the change in ΔAE mean latency was revealed.

unpaired testing revealed a significantly larger change in CBF in the EXP group compared with the CON group in several regions: bilateral inferior parietal lobule, the left inferior frontal gyrus, superior parietal lobule, middle temporal gyrus, ACC and precentral gyrus, as well as the right fusiform gyrus (Fig. 13).

4. Discussion

The study presented in this work trained down-regulation of the auditory cortex using fMRI-NFT and directed attention strategies. Such a technique may be applicable to the treatment of neurologic disorders such as tinnitus. The experimental group attempted self-regulation with the aid of real information regarding the current BOLD signals in the AC while the control group was supplied sham feedback yoked from a random participant in the experimental group and matched for training progress. In both groups, the bilateral AC was identified both anatomically and functionally using an activation map produced during binaural continuous noise stimulation at each of the five training sessions. The results indicate an overall increase in the ability to volitionally decrease AC activity across training, a region known to be hyperactive in chronic tinnitus. Activation changes in other regions during closed-loop endogenous neuromodulation were also observed much of the frontal cortex, and anterior cingulate indicating the involvement of attentional and monitoring processes. The frontal cortex and anterior cingulate are likely involved with auditory attention processes (Roberts et al., 2013). Control over AC de-activation was not found to be significantly different at the first session between the experimental and control groups. However, the ability to volitionally decrease AC activity was observed to be significantly greater for the experimental group compared to the control group at sessions two and five. Furthermore, self-control over AC de-activation between the first and last training session was significantly increased in the experimental group. There was also a significant increase between the first and second training session signifying a rapid effect of neurofeedback training on AC control. These effects were not observed in the control group.

These results add to a growing body of research that demonstrates the success of fMRI-NFT in teaching individuals to self-regulate localized brain activity. A previous controlled study indicates healthy individuals can learn to control the activated cortical volume in the primary and secondary auditory cortex using fMRI-NFT (Yoo et al., 2006). A second previous study indicated that control over the magnitude of A1 activation is also achievable however not necessarily attributable to fMRI-NFT (Haller et al., 2010). A third previous study implication the possibility

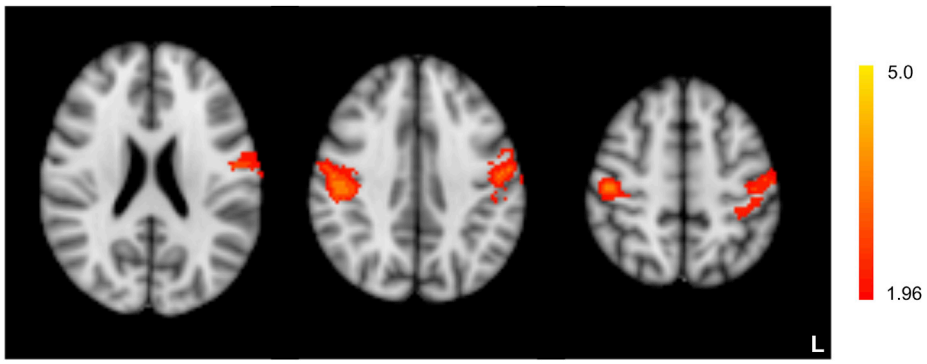

Fig. 11. *F* test results for the main effect of session indicate increased activation in the precentral and postcentral gyri across training in response to binaural auditory stimulation. Axial slices are displayed at MNI coordinates z = 22, 38, and 52 mm (left to right).

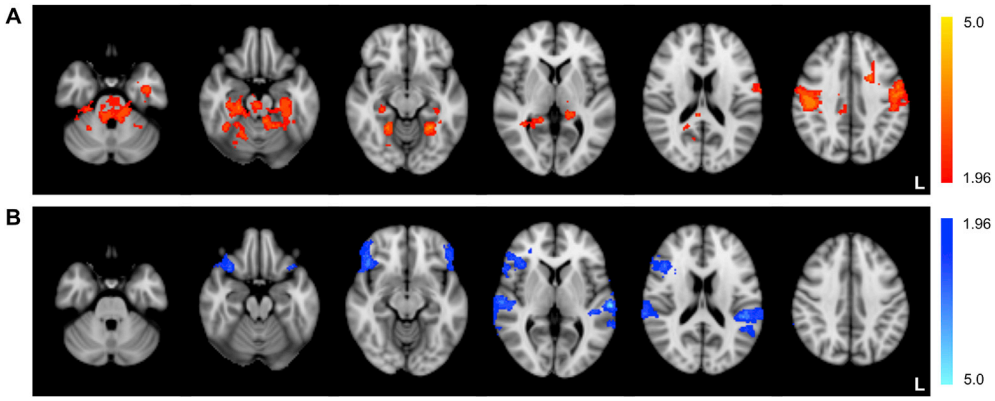

Fig. 12. Contrast identifying voxels with significantly increased (A) and decreased (B) activation across training in response to binaural auditory stimulation. Axial slices are displayed at MNI coordinates z = −30, −20, −12, 4, 18, and 38 mm (left to right).

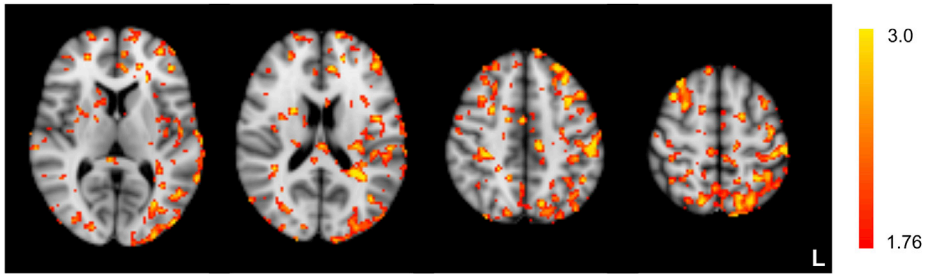

Fig. 13. Differential changes in cerebral perfusion across fMRI-NFT between groups. Axial slices are displayed at MNI coordinates z = 8, 18, 46, and 56 mm (left to right).

of tinnitus patients to down-regulate the auditory cortex using continuous and intermittent neurofeedback (Emmert et al., 2017a). Single-session results identified greater down-regulation in the intermittent feedback group; but over multiple sessions, the continuous feedback was more advantageous. The results above support the previous finding that fMRI-NFT aids control over the magnitude of AC de-activation, and this capability can be trained in the presence of sound. Moreover, this result shows that 60 min of distributed fMRI-NFT is adequate to train AC self-regulation, but significant observable effects are prevalent within 24 min of training.

Training self-regulation of brain activity from fMRI-NFT has shown promise in a broad range of applications such as the improvement of human performance (Scharnowski et al., 2012; Sherwood et al., 2016a; Zhang et al., 2013) and a variety of medical applications including recovery from stroke (Chiew et al., 2012; Liew et al., 2015), major depression (Linden et al., 2012; Mehler et al., 2018; Young et al., 2014; Yuan et al., 2014), Parkinson's disease (Subramanian et al., 2011), and chronic pain (deCharms et al., 2005; Emmert et al., 2017b; Zhang et al., 2018). However, only a few previous studies have investigated fMRI-NFT as a possible treatment for tinnitus (Emmert et al., 2017a; Haller et al., 2010; Yoo et al., 2006).

Moreover, this work evaluated the neural and behavioral implications by assessing the impact of fMRI-NFT on attentional processes. The results of the work presented herein do suggest improved control over the activity of the AC did lead to decreased distractibility (*i.e.,* increased attentional control), a result that did not survive when the groups were separated. This finding implies that attempting volitional down-regulation of the AC may alter distractibility and attentional control. This research also measured changes in neural processes associated with fMRI-NFT. The results of this work identified a significant reduction in AC activity in response to binaural continuous noise stimulation. Due to this effect being prevalent across both experimental and control groups,

it may be a training effect or stimulus adaptation; however, it is also plausible that this effect is from attempted down-regulation of auditory activity. Unfortunately, this research lacks the ability to differentiate these effects. It should be noted that our use of a task-based white noise paradigm with continuous scanning may not have been optimal for mapping of the AC, and this may have impacted our ability to find an interaction effect in the AC localization procedure across sessions. Our design was chosen to keep the fMRI and NFT sequences as similar as possible and to minimize differences in AC response associated with individual tonal-specific hearing differences, which were not controlled.

Similarly, differential changes in resting cerebral perfusion were observed across training between the groups. Due to the infancy of ASL and that it has yet to be clearly quantitatively validated, these findings should be interpreted cautiously. Xu et al. (2010) found a high reliability of perfusion measures in 3D pcASL measurements of perfusion in both young and older subjects. Futher, they found agreement between measurements of perfusion between 3D pcASL and ^{15}O-water positron emission tomography in older individuals. However, we have implemented ASL in the methodology set forth by Alsop et al. (2015) which describes the optimal default implementation for clinical applications resulting from a consensus of the ISMRM Perfusion Study Group that was reached in October 2012.

Finally, this study has many limitations which may impact the interpretation of the findings. First and foremost, the differential sample sizes between our control (n = 9) and experimental (n = 18) groups. Unequal sample sizes can affect the homogeneity of variance assumptions and power. Due to power being computed from the smallest sample size, the disproportionate grouping should have decreased our ability to observe significant effects between the experimental and control groups. Despite this, there were significant effects observed in several measures. The unequal groups was part of our design to make best use of the project funds while accounting for future portions of the funded effort. Another limitation is that our participants were healthy. While our funding and effort is focused on tinnitus, this particular study was really focused on utilizing an existing fMRI-NFT paradigm (left prefrontal cortex) to see if activity of a different brain region (auditory cortex) can be down-regulated while concurrently providing auditory stimulation. With deactivation of a new brain region being the main focus, other measures (*e.g.*, behavioral) were secondary and could have been more robustly developed and applied. However, to reiterate, our goal was to show that our neurofeedback approach successfully enabled participants to control activity in their auditory cortex. This region and down-regulation were specifically chosen due to the hyperactivity of the auditory cortex that has been associated with tinnitus patients (Gu et al., 2010; Langguth et al., 2006; Schecklmann et al., 2013; Seydell-Greenwald et al., 2012; Wang et al., 2001). A third limitation was the single-blinded nature of this study where only the participants were blinded to the grouping. Originally, we designed the control condition differently and in such a way that double-blinding was not possible. After piloting, we determined this method was flawed and implemented the method presented in this paper without adding blinding to the researchers. Single-blinded studies may cause researchers to inadvertently place unequal demand characteristics on the groups leading to downstream differences in behavior and brain activity (Thibault et al., 2018). A further limitation is the absence of accounting for respiration artifacts (*e.g.,* respiration volume and heart rate variability) which can significantly alter the BOLD signal or provide the experimental group, but not control group, with a form of respiration biofeedback that may help them achieve self-regulation (Thibault et al., 2018).

5. Conclusion

The results presented in this work align with previous findings which indicate fMRI-NFT can teach control over the auditory cortex. However, the results of the presented work add to the previous findings by indicating volitional down-regulation of the auditory cortex is achievable using fMRI-NFT, and that this control is possible in the presence of continuous noise. Our findings suggest future work should evaluate the efficacy of attempting down-regulation of the auditory cortex in the presence of binaural auditory stimulation in a cohort of tinnitus patients. Tinnitus is a neurologic disorder associated with hyperactivity of the auditory cortex and reduced attentional control leading to increased attention directed towards the auditory system. This is exacerbated by enhanced emotional responses to auditory stimuli. Tinnitus can cause severe impairments and may even limit the ability to perform daily functions. The number of U.S. veterans receiving service-connected disability compensation for tinnitus exceeds all other compensation receipient disabilities including post-traumatic stress disorder, hearing loss, and lumbosacral or cervical strain. Although this work demonstrated fMRI-NFT aided the ability to control the auditory cortex, the findings were not limited to the group which received real neurofeedback. These findings represent the possibility of such a treatment to be transitioned outside of the MRI to possible home-based therapies which may be provided through mobile applications or simple to use devices.

Conflicts of interest

The authors declare that this research was conducted in the absence of any commercial or financial relationships that could be construed as a potential conflict of interest.

Acknowledgements

This material is based on research sponsored by the U.S. Air Force under agreement number FA8650-16-2-6702. The views expressed are those of the authors and do not reflect the official views or policy of the Department of Defense and its Components. The U.S. Government is authorized to reproduce and distribute reprints for Governmental purposes notwithstanding any copyright notation thereon. The voluntary, fully informed consent of the subjects used in this research was obtained as required by 32 CFR 219 and DODI 3216.02_AFI 40–402.

Appendix A. Supplementary data

Supplementary data to this article can be found online at https://doi.org/10.1016/j.neuroimage.2019.03.078.

References

Alsop, D.C., Detre, J.A., 1996. Reduced transit-time sensitivity in noninvasive magnetic resonance imaging of human cerebral blood flow. J. Cereb. Blood Flow Metab. 16, 1236–1249. https://doi.org/10.1097/00004647-199611000-00019.

Alsop, D.C., Detre, J.A., Golay, X., Günther, M., Hendrikse, J., Hernandez-Garcia, L., Lu, H., MacIntosh, B.J., Parkes, L.M., Smits, M., van Osch, M.J.P., Wang, D.J.J., Wong, E.C., Zaharchuk, G., 2015. Recommended implementation of arterial spin-labeled perfusion MRI for clinical applications: a consensus of the ISMRM perfusion study group and the European consortium for ASL in dementia. Magn. Reson. Med. 73, 102–116. https://doi.org/10.1002/mrm.25197.

Anderson, M.J., Robinson, J., 2001. Permutation tests for linear models. Aust. N. Z. J. Stat. 43, 75–88. https://doi.org/10.1111/1467-842X.00156.

Ashby, F.G., 2011. Statistical Analysis of fMRI Data. MIT press.

Caria, A., Veit, R., Sitaram, R., Lotze, M., Weiskopf, N., Grodd, W., Birbaumer, N., 2007. Regulation of anterior insular cortex activity using real-time fMRI. Neuroimage 35, 1238–1246. https://doi.org/10.1016/j.neuroImage.2007.01.018.

Chen, W.J., Hsiao, C.K., Hsiao, L.-L., Hwu, H.-G., 1998. Performance of the continuous performance test among community samples. Schizophr. Bull. 24, 163–174. https://doi.org/10.1093/oxfordjournals.schbul.a033308.

Chiew, M., LaConte, S.M., Graham, S.J., 2012. Investigation of fMRI neurofeedback of differential primary motor cortex activity using kinesthetic motor imagery. Neuroimage 61, 21–31. https://doi.org/https://doi.org/10.1016/j.neuroImage.2012.02.053.

Collins, D.L., Holmes, C.J., Peters, T.M., Evans, A.C., 1995. Automatic 3-D model-based neuroanatomical segmentation. Hum. Brain Mapp. 3, 190–208. https://doi.org/10.1002/hbm.460030304.

Cox, R.W., Jesmanowicz, A., Hyde, J.S., 1995. Real-time functional magnetic resonance imaging. Magn. Reson. Med. 33, 230–236. https://doi.org/10.1002/mrm.1910330213.

deCharms, R.C., Maeda, F., Glover, G.H., Ludlow, D., Pauly, J.M., Soneji, D., Gabrieli, J.D.E., Mackey, S.C., 2005. Control over brain activation and pain learned

by using real-time functional MRI. Proc. Natl. Acad. Sci. U. S. A 102, 18626–18631. https://doi.org/10.1073/pnas.0505210102.
Derryberry, D., Reed, M.A., 2002. Anxiety-related attentional biases and their regulation by attentional control. J. Abnorm. Psychol. 111 (2), 225–236. https://doi.org/10.1037/0021-843X.111.2.225.
Dixon, W.T., Sardashti, M., Castillo, M., Stomp, G.P., 1991. Multiple inversion recovery reduces static tissue signal in angiograms. Magn. Reson. Med. 18, 257–268. https://doi.org/10.1002/mrm.1910180202.
Emmert, K., Kopel, R., Koush, Y., Maire, R., Senn, P., Van De Ville, D., Haller, S., 2017a. Continuous vs. Intermittent neurofeedback to regulate auditory cortex activity of tinnitus patients using real-time fMRI – a pilot study. NeuroImage Clin 14, 97–104. https://doi.org/10.1016/j.nicl.2016.12.023.
Emmert, K., Breimhorst, M., Bauermann, T., Birklein, F., Rebhorn, C., Van De Ville, D., Haller, S., 2017b. Active pain coping is associated with the response in real-time fMRI neurofeedback during pain. Brain Imaging Behav 11 (3), 712–721. https://doi.org/10.1007/s11682-016-9547-0.
Fera, F., Yongbi, M.N., van Gelderen, P., Frank, J.A., Mattay, V.S., Duyn, J.H., 2003. EPI-BOLD fMRI of human motor cortex at 1.5 T and 3.0 T: Sensitivity dependence on echo time and acquisition bandwidth. J. Magn. Reson. Imaging 19, 19–26. https://doi.org/10.1002/jmri.10440.
Folmer, R.L., Theodoroff, S.M., Martin, W.H., Shi, Y., 2014. Experimental, controversial, and futuristic treatments for chronic tinnitus. J. Am. Acad. Audiol. 25, 106–125. https://doi.org/10.3766/jaaa.25.1.7.
Friston, K.J., Holmes, A.P., Poline, J.-B., Grasby, P.J., Williams, S.C.R., Frackowiak, R.S.J., Turner, R., 1995. Analysis of fMRI time-series revisited. Neuroimage 2, 45–53. https://doi.org/10.1006/nimg.1995.1007.
Glover, G.H., 2012. Spiral imaging in fMRI. Neuroimage 62, 706–712. https://doi.org/10.1016/J.NEUROIMAGE.2011.10.039.
Green, D.M., Swets, J.A., 1966. Signal Detection Theory and Psychophysics. Wiley, New York, NY.
Greve, D.N., Fischl, B., 2009. Accurate and robust brain image alignment using boundary-based registration. Neuroimage 48, 63–72. https://doi.org/10.1016/j.neuroImage.2009.06.060.
Gu, J.W., Halpin, C.F., Nam, E.-C., Levine, R.A., Melcher, J.R., 2010. Tinnitus, diminished sound-level tolerance, and elevated auditory activity in humans with clinically normal hearing sensitivity. J. Neurophysiol. 104, 3361–3370.
Halford, J.B.S., Anderson, S.D., 1991. Anxiety and depression in tinnitus sufferers. J. Psychosom. Res. 35, 383–390. https://doi.org/10.1016/0022-3999(91)90033-K.
Haller, S., Birbaumer, N., Veit, R., 2010. Real-time fMRI feedback training may improve chronic tinnitus. Eur. Radiol. 20, 696–703. https://doi.org/10.1007/s00330-009-1595-z.
Hamilton, J.P., Glover, G.H., Hsu, J.-J., Johnson, R.F., Gotlib, I.H., 2011. Modulation of subgenual anterior cingulate cortex activity with real-time neurofeedback. Hum. Brain Mapp. 32, 22–31. https://doi.org/10.1002/hbm.20997.
Harris, C.R., Pashler, H., 2004. Attention and the processing of emotional words and names: not so special after all. Psychol. Sci. 15, 171–178. https://doi.org/10.1111/j.0956-7976.2004.01503005.x.
Hyde, J.S., Biswal, B.B., Jesmanowicz, A., 2001. High-resolution fMRI using multislice partial k-space GR-EPI with cubic voxels. Magn. Reson. Med. 46, 114–125. https://doi.org/10.1002/mrm.1166.
Jenkinson, M., Bannister, P., Brady, M., Smith, S., 2002. Improved optimization for the robust and accurate linear registration and motion correction of brain images. Neuroimage 17, 825–841. https://doi.org/10.1006/nimg.2002.1132.
Jenkinson, M., Smith, S., 2001. A global optimisation method for robust affine registration of brain images. Med. Image Anal. 5, 143–156. https://doi.org/10.1016/S1361-8415(01)00036-6.
Johnston, S., Linden, D.E.J., Healy, D., Goebel, R., Habes, I., Boehm, S.G., 2011. Upregulation of emotion areas through neurofeedback with a focus on positive mood. Cognit. Affect Behav. Neurosci. 11, 44–51. https://doi.org/10.3758/s13415-010-0010-1.
Jun, H.J., Park, M.K., 2013. Cognitive behavioral therapy for tinnitus: evidence and efficacy. Korean J. Audiol. 17, 101–104. https://doi.org/10.7874/kja.2013.17.3.101.
Langers, D.R.M., Krumbholz, K., Bowtell, R.W., Hall, D.A., 2014a. Neuroimaging paradigms for tonotopic mapping (I): the influence of sound stimulus type. Neuroimage 100, 650–662. https://doi.org/10.1016/J.NEUROIMAGE.2014.07.044.
Langers, D.R.M., Sanchez-Panchuelo, R.M., Francis, S.T., Krumbholz, K., Hall, D.A., 2014b. Neuroimaging paradigms for tonotopic mapping (II): the influence of acquisition protocol. Neuroimage 100, 663–675. https://doi.org/10.1016/J.NEUROIMAGE.2014.07.042.
Langers, D.R.M., van Dijk, P., 2011. Robustness of intrinsic connectivity networks in the human brain to the presence of acoustic scanner noise. Neuroimage 55, 1617–1632. https://doi.org/10.1016/J.NEUROIMAGE.2011.01.019.
Langguth, B., Eichhammer, P., Kreutzer, A., Maenner, P., Marienhagen, J., Kleinjung, T., Sand, P., Hajak, G., 2006. The impact of auditory cortex activity on characterizing and treating patients with chronic tinnitus – first results from a PET study. Acta Otolaryngol. 126, 84–88. https://doi.org/10.1080/03655230600895317.
Liew, S.-L., Rana, M., Cornelsen, S., Fortunato de Barros Filho, M., Birbaumer, N., Sitaram, R., Cohen, L.G., Soekadar, S.R., 2015. Improving motor corticothalamic communication after stroke using real-time fMRI connectivity-based neurofeedback. Neurorehabilitation Neural Repair 30, 671–675. https://doi.org/10.1177/1545968315619699.
Linden, D.E.J., Habes, I., Johnston, S.J., Linden, S., Tatineni, R., Subramanian, L., Sorger, B., Healy, D., Goebel, R., 2012. Real-time self-regulation of emotion networks in patients with depression. PLoS One 7, e38115. https://doi.org/10.1371%2Fjournal.pone.0038115.
Lovie, P., 1986. Identifying outliers. In: Lovie, A.D. (Ed.), New Developments in Statistics for Psychology and the Social Sciences. The British Psychological Society and Metheun, London, UK, pp. 44–69.
Mak, J.N., Wolpaw, J.R., 2009. Clinical applications of brain-computer interfaces: current state and future prospects. Biomed. Eng. IEEE Rev. 2, 187–199. https://doi.org/10.1109/RBME.2009.2035356.
Mani, S., Pauly, J., Conolly, S., Meyer, C., Nishimura, D., 1997. Background suppression with multiple inversion recovery nulling: applications to projective angiography. Magn. Reson. Med. 37, 898–905. https://doi.org/10.1002/mrm.1910370615.
Mazziotta, J., Toga, A., Evans, A., Fox, P., Lancaster, J., Zilles, K., Woods, R., Paus, T., Simpson, G., Pike, B., Holmes, C., Collins, L., Thompson, P., MacDonald, D., Iacoboni, M., Schormann, T., Amunts, K., Palomero-Gallagher, N., Geyer, S., Parsons, L., Narr, K., Kabani, N., Goualher, G. Le, Boomsma, D., Cannon, T., Kawashima, R., Mazoyer, B., 2001. A probabilistic atlas and reference system for the human brain: international Consortium for Brain Mapping (ICBM). Philos. Trans. R. Soc. London.Series B Biol. Sci. 356, 1293–1322. https://doi.org/10.1098/rstb.2001.0915.
Mehler, D.M.A., Sokunbi, M.O., Habes, I., Barawi, K., Subramanian, L., Range, M., Evans, J., Hood, K., Lührs, M., Keedwell, P., Goebel, R., Linden, D.E.J., 2018. Targeting the affective brain—a randomized controlled trial of real-time fMRI neurofeedback in patients with depression. Neuropsychopharmacology 43, 2578–2585. https://doi.org/10.1038/s41386-018-0126-5.
Moray, N., 1959. Attention in dichotic listening: affective cues and the influence of instructions. Q. J. Exp. Psychol. 11, 56–60. https://doi.org/10.1080/17470215908416289.
Mutsaerts, H.J.M.M., Steketee, R.M.E., Heijtel, D.F.R., Kuijer, J.P.A., van Osch, M.J.P., Majoie, C.B.L.M., Smits, M., Nederveen, A.J., 2014. Inter-vendor reproducibility of pseudo-continuous arterial spin labeling at 3 tesla. PLoS One 9, e104108. https://doi.org/10.1371/journal.pone.0104108.
Nichols, T., Holmes, A., 2003. Nonparametric permutation tests for functional NeuroImaging. In: Human Brain Function, second ed., pp. 887–910 https://doi.org/10.1016/B978-012264841-0/50048-2.
Patriat, R., Molloy, E.K., Meier, T.B., Kirk, G.R., Nair, V.A., Meyerand, M.E., Prabhakaran, V., Birn, R.M., 2013. The effect of resting condition on resting-state fMRI reliability and consistency: a comparison between resting with eyes open, closed, and fixated. Neuroimage 78, 463–473. https://doi.org/10.1016/j.neuroImage.2013.04.013.
Roberts, L.E., Husain, F.T., Eggermont, J.J., 2013. Role of attention in the generation and modulation of tinnitus. Neurosci Bopbehav Rev 37, 1754–1773. https://doi.org/10.1016/j.neubiorev.2013.07.007.
Saliba, J., Al-Reefi, M., Carriere, J.S., Verma, N., Provencal, C., Rappaport, J.M., 2016. Accuracy of mobile-based audiometry in the evaluation of hearing loss in quiet and noisy environments. Otolaryngol. Neck Surg. 156, 706–711. https://doi.org/10.1177/0194599816683663.
Scharnowski, F., Hutton, C., Josephs, O., Weiskopf, N., Rees, G., 2012. Improving visual perception through neurofeedback. J. Neurosci. 32, 17830–17841. https://doi.org/10.1523/JNEUROSCI.6334-11.2012.
Schecklmann, M., Landgrebe, M., Poeppl, T.B., Kreuzer, P., Männer, P., Marienhagen, J., Wack, D.S., Kleinjung, T., Hajak, G., Langguth, B., 2013. Neural correlates of tinnitus duration and Distress: a positron emission tomography study. Hum. Brain Mapp. 34, 233–240.
Seydell-Greenwald, A., Leaver, A.M., Turesky, T.K., Morgan, S., Kim, H.J., Rauschecker, J.P., 2012. Functional MRI evidence for a role of ventral prefrontal cortex in tinnitus. Adv. Neurosci. Tinnitus 1485, 22–39. https://doi.org/https://doi.org/10.1016/j.brainres.2012.08.052.
Sherwood, M.S., Kane, J.H., Weisend, M.P., Parker, J.G., 2016a. Enhanced control of dorsolateral prefrontal cortex neurophysiology with real-time functional magnetic resonance imaging (rt-fMRI) neurofeedback training and working memory practice. Neuroimage 124, 214–223. https://doi.org/10.1016/j.neuroImage.2015.08.074.
Sherwood, M.S., Weisend, M.P., Kane, J.H., Parker, J.G., 2016b. Combining real-time fMRI neurofeedback training of the DLPFC with *n*-back practice results in neuroplastic effects confined to the neurofeedback target region. Front. Behav. Neurosci. 10 (138), 1–9. https://doi.org/10.3389/fnbeh.2016.00138.
Shinozaki, J., Harada, K., Nagahama, H., Sakurai, Y., Akatsuka, Y., Nagamine, T., Kochiyama, T., 2013. In the range of 20 to 35ms, an echo-time of 20ms is preferred for 3-tesla functional magnetic resonance imaging. Adv. Biomed. Eng. 2, 47–54. https://doi.org/10.14326/abe.2.47.
Silva, A.C., Kim, S.-G., 1999. Pseudo-continuous arterial spin labeling technique for measuring CBF dynamics with high temporal resolution. Magn. Reson. Med. 42, 425–429. https://doi.org/10.1002/(SICI)1522-2594(199909)42:3<425::AID-MRM3>3.0.CO;2-S.
Smith, S.M., 2002. Fast robust automated brain extraction. Hum. Brain Mapp. 17, 143–155. https://doi.org/10.1002/hbm.10062.
Smith, S.M., Jenkinson, M., Woolrich, M.W., Beckmann, C.F., Behrens, T.E.J., Johansen-Berg, H., Bannister, P.R., De Luca, M., Drobnjak, I., Flitney, D.E., Niazy, R.K., Saunders, J., Vickers, J., Zhang, Y., De Stefano, N., Brady, J.M., Matthews, P.M., 2004. Advances in functional and structural MR image analysis and implementation as FSL. Neuroimage 23, S208–S219. https://doi.org/10.1016/j.neuroImage.2004.07.051.
Sorkin, R.D., 1999. Spreadsheet signal detection. Behav. Res. Methods Instrum. Comput. 31, 46–54. https://doi.org/10.3758/BF03207691.
Subramanian, L., Hindle, J.V., Johnston, S., Roberts, M.V., Husain, M., Goebel, R., Linden, D., 2011. Real-time functional magnetic resonance imaging neurofeedback for treatment of Parkinson's disease. J. Neurosci. 31, 16309–16317. https://doi.org/10.1523/JNEUROSCI.3498-11.2011.

Sulzer, J., Haller, S., Scharnowski, F., Weiskopf, N., Birbaumer, N., Blefari, M.L., Bruehl, A.B., Cohen, L.G., DeCharms, R.C., Gassert, R., Goebel, R., Herwig, U., LaConte, S., Linden, D., Luft, A., Seifritz, E., Sitaram, R., 2013. Real-time fMRI neurofeedback: progress and challenges. Neuroimage 76, 386–399. https://doi.org/10.1016/j.neuVroImage.2013.03.033.

Swets, J.A., Sewall, S.T., 1963. Invariance of signal detectability over stages of practice and levels of motivation. J. Exp. Psychol. 66, 120–126. https://doi.org/10.1037/h0049098.

Thibault, R.T., MacPherson, A., Lifshitz, M., Roth, R.R., Raz, A., 2018. Neurofeedback with fMRI: a critical systematic review. Neuroimage 172, 786–807. https://doi.org/10.1016/j.neuroimage.2017.12.071.

Thompson, G.P., Sladen, D.P., Borst, B.J.H., Still, O.L., 2015. Accuracy of a tablet audiometer for measuring behavioral hearing thresholds in a clinical population. Otolaryngol. Neck Surg. 153, 838–842. https://doi.org/10.1177/0194599815593737.

Vaughan, T.M., McFarland, D.J., Schalk, G., Sarnacki, W.A., Krusienski, D.J., Sellers, E.W., Wolpaw, J.R., 2006. The wadsworth BCI research and development program: at home with BCI. Neural Syst. Rehabil. Eng. IEEE Trans. 14, 229–233. https://doi.org/10.1109/TNSRE.2006.875577.

Veit, R., Singh, V., Sitaram, R., Caria, A., Rauss, K., Birbaumer, N., 2012. Using real-time fMRI to learn voluntary regulation of the anterior insula in the presence of threat-related stimuli. Soc. Cognit. Affect Neurosci. 7, 623–634. https://doi.org/10.1093/scan/nsr061.

Wager, T.D., Lindquist, M.A., 2011. Essentials of functional magnetic resonance imaging. In: Decety, J., Cacioppo, J.T. (Eds.), The Oxford Handbook of Social Neuroscience. Oxford University Press, pp. 69–96.

Wang, H., Tian, J., Yin, D., Jiang, S., Yang, W., Han, D., Yao, S., Shao, M., 2001. Regional glucose metabolic increases in left auditory cortex in tinnitus patients: a preliminary study with positron emission tomography. Chin. Med. J. 114, 848–851.

Weiskopf, N., Sitaram, R., Josephs, O., Veit, R., Scharnowski, F., Goebel, R., Birbaumer, N., Deichmann, R., Mathiak, K., 2007. Real-time functional magnetic resonance imaging: methods and applications. Proc. Int. Sch. Magn. Reson. Brain Funct. Proc. Int. Sch. Magn. Reson. Brain Funct. 25, 989–1003. https://doi.org/10.1016/j.mri.2007.02.007.

Winkler, A.M., Ridgway, G.R., Webster, M.A., Smith, S.M., Nichols, T.E., 2014. Neuroimage 92, 381–397. https://doi.org/10.1016/J.NEUROIMAGE.2014.01.060.

Woolrich, M.W., Jbabdi, S., Patenaude, B., Chappell, M., Makni, S., Behrens, T., Beckmann, C., Jenkinson, M., Smith, S.M., 2009. Bayesian analysis of neuroImaging data in FSL. Neuroimage 45, S173–S186. https://doi.org/10.1016/j.neuroImage.2008.10.055.

Xu, G., Rowley, H.A., Wu, G., Alsop, D.C., Shankaranarayanan, A., Dowling, M., Christian, B.T., Oakes, T.R., Johnson, S.C., 2010. Reliability and precision of pseudo-continuous arterial spin labeling perfusion MRI on 3.0 T and comparison with ^{15}O-water PET in elderly subjects at risk for alzheimer's disease. NMR Biomed. 23, 286–293. https://doi.org/10.1002/nbm.1462.

Ye, F.Q., Frank, J.A., Weinberger, D.R., McLaughlin, A.C., 2000. Noise reduction in 3D perfusion imaging by attenuating the static signal in arterial spin tagging (ASSIST). Magn. Reson. Med. 44, 92–100. https://doi.org/10.1002/1522-2594(200007)44:1<92::AID-MRM14>3.0.CO;2-M.

Yoo, S.-S., O'Leary, H.M., Fairneny, T., Chen, N.-K., Panych, L.P., Park, H., Jolesz, F.A., 2006. Increasing cortical activity in auditory areas through neurofeedback functional magnetic resonance imaging. Neuroreport 17, 1273–1278.

Young, K.D., Zotev, V., Phillips, R., Misaki, M., Yuan, H., Drevets, W.C., Bodurka, J., 2014. Real-time fMRI neurofeedback training of amygdala activity in patients with major depressive disorder. PLoS One 9, e88785.

Yuan, H., Young, K.D., Phillips, R., Zotev, V., Misaki, M., Bodurka, J., 2014. Resting-state functional connectivity modulation and sustained changes after real-time functional magnetic resonance imaging neurofeedback training in depression. Brain Connect. 4, 690–701. https://doi.org/10.1089/brain.2014.0262.

Zhang, G., Yao, L., Zhang, H., Long, Z., Zhao, X., 2013. Improved working memory performance through self-regulation of dorsal lateral prefrontal cortex activation using real-time fMRI. PLoS One 8, e73735. https://doi.org/10.1371/journal.pone.0073735.

Zhang, S., Yoshida, W., Mano, H., Yanagisawa, T., Shibata, K., Kawato, M., Seymour, B., 2018. Endogenous controllability of closed-loop brain-machine interfaces for pain. bioRxiv. https://doi.org/10.1101/369736.